

Spin Order and Excitations in Triangular Antiferromagnet $\text{La}_2\text{Ca}_2\text{MnO}_7$

Wei Bao,^{1,*} Y.X. Wang,^{2,†} Y. Qiu,^{3,4} K. Li,² J.H. Lin,²
J.R.D. Copley,³ R.W. Erwin,³ B.S. Dennis,⁵ and A.P. Ramirez^{6,5}

¹*Department of Physics, Renmin University of China, Beijing 100872, China*

²*Beijing National Laboratory for Molecular Sciences, State Key Laboratory of Rare Earth Materials Chemistry and Applications, College of Chemistry, Peking University, Beijing 100871, China*

³*NIST Center for Neutron Research, National Institute of Standards and Technology, Gaithersburg, MD 20899, USA*

⁴*Dept. of Materials Science and Engineering, University of Maryland, College Park, MD 20742, USA*

⁵*Bell Laboratories, Alcatel-Lucent, Murray Hill, NJ 07974, USA*

⁶*Baskin School of Engineering, University of California, Santa Cruz, CA 95060, USA*

(Dated: November 5, 2018)

We report a spin $S = 3/2$ triangular antiferromagnet with nearest-neighbor coupling $J = 0.29$ meV in $\text{La}_2\text{Ca}_2\text{MnO}_7$. A genuinely two-dimensional, three-sublattice $\sqrt{3} \times \sqrt{3}$ order develops below $T_N = 2.80$ K $\ll |\Theta| = 25$ K. The spin excitations deviate substantially from linear spin-wave theory, suggesting that magnon breakdown occurs in the material. Such a breakdown has been anticipated in recent theoretical studies, although the excitation spectrum remains to be accounted for.

PACS numbers: 75.25.+z, 78.70.Nx, 75.10.Jm, 75.30.-m

It is well known that quantum fluctuations renormalize Néel order only moderately in three dimensions (3D)[1], but prevent completely the long-range order even at $T = 0$ for 1D spin systems with short-range antiferromagnetic coupling[2]. In 2D, the quantum antiferromagnet can be either long-range ordered or remain a quantum liquid at 0 K, depending on the local geometry. The interplay of geometric frustration and quantum fluctuations forms a frontier research area in many-body physics[3].

It has long been established that a 2D Ising system, which is not quantum, has a finite-temperature transition to long-range order[4]. When spins have continuous symmetry, no long-range order is possible above zero temperature as dictated by the Mermin-Wagner theorem[5], although a critical state with power-law correlations and divergent magnetic susceptibility exists below the finite-temperature Kosterlitz-Thouless transition[6]. At zero temperature, Néel order is stable on a square lattice[7]. However, bipartite Néel order is not possible on a triangular or kagome lattice. This effect of geometrical frustration[3] promises to tip the balance towards a quantum spin liquid, such as the resonating-valence-bond (RVB) state proposed by Anderson[8]. On the other hand, a generalized Néel order, the three-sublattice $\sqrt{3} \times \sqrt{3}$ state (Fig. 1b), has also been proposed as the ground state[9]. In this state, neighboring spins are oriented at 120° to each other, thereby partially relaxing the geometrical frustration. The ground state of the 2D quantum antiferromagnet on the strongly frustrated kagome lattice is believed to be a quantum spin liquid. On the triangular lattice, the spin-half RVB and $\sqrt{3} \times \sqrt{3}$ states are so close in energy that it has taken three decades of extensive theoretical investigation for a consensus to emerge that favors the $\sqrt{3} \times \sqrt{3}$ state[7, 10].

Close to the order-disorder phase boundary of quantum spin systems, the triangular antiferromagnet (TAF)

holds a special place in the study of quantum fluctuation effects. However, compounds that approximate the ideal situation of the theoretical model are rare. The initially studied TAF materials are dominated by interlayer interaction, thus quasi-1D[11]. Among quasi-2D materials, there was difficulty in realizing a true triangular lattice with identical nearest neighbor coupling, or without significant interaction beyond nearest neighbors in the plane, a situation which leads to different ground states[12]. When the nearest-neighbor interaction dominates on a triangular lattice and leads to the correct $\sqrt{3} \times \sqrt{3}$ order in VX_2 ($X = \text{Cl, Br or I}$)[13], XCrO_2 ($X = \text{Li, Na or Cu}$)[14, 15], $\text{XFe(SO}_4)_2$ ($X = \text{Cs or Rb}$)[16] and $\text{RbFe(MoO}_4)_2$ [17], such materials develop 3D order due to nonzero interplane magnetic interactions, and 2D quantum physics is suppressed. In this work we show that the new triangular lattice compound $\text{La}_2\text{Ca}_2\text{MnO}_7$ does not suffer from any of these problems, and exhibits novel ground state behavior down to 0.04 K.

The structure of $\text{La}_2\text{Ca}_2\text{MnO}_7$ is comprised of alternate hexagonal perovskite La_2MnO_6 and graphite-like Ca_2O sublayers (Fig. 1a), as determined by the combined neutron and x-ray diffraction study[18]. The lattice parameters are $a = 5.619\text{\AA}$ and $c = 17.292\text{\AA}$ at 40 mK. Magnetism is associated with the Mn^{4+} ions inside the MnO_6 octahedra which form a perfect triangular lattice demanded by the $R\bar{3}m$ space group symmetry[18]. The close-packed ABC stacking of triangular layers cancels possible interlayer exchange coupling due to the zero summation of the $\sqrt{3} \times \sqrt{3}$ -ordered magnetic moments in a triangle (Fig. 1b). The half-filled t_{2g}^3 electronic configuration of Mn^{4+} has spin $S = 3/2$, and the magnetic susceptibility above 9 K is well described by the Rushbrooke-Wood formulas for TAF[19] with the nearest-neighbor exchange $J = 0.29$ meV and the Weiss temperature $\Theta \equiv -2JS(S+1)/k = -25$ K. Heat capacity mea-

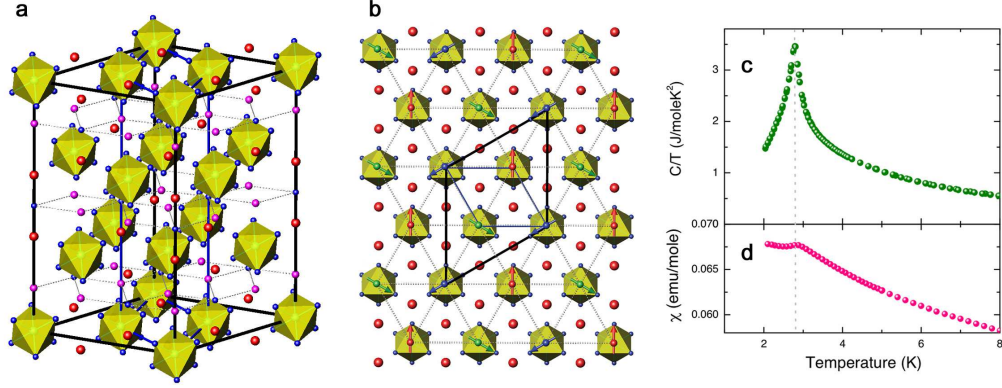


FIG. 1: (color online) (a) A magnetic unit cell of $\text{La}_2\text{Ca}_2\text{MnO}_7$, which contains three triangular layers with the corner of a triangle stacking in the center of the triangles in the neighboring layers in the close-packed ABC sequence. The red balls represent La, the pink Ca, the blue O ions. (b) Top view of La_2MnO_6 . The spins of the Mn^{4+} ions in the centers of the MnO_6 octahedra form a triangular lattice, and the arrows depict the $\sqrt{3} \times \sqrt{3}$ antiferromagnetic order with three color-coded spin sublattices. The magnetic unit cell (black lines) is three times larger than the structural unit cell (blue lines). (c) Specific heat divided by temperature, as a function of temperature. (d) Magnetic susceptibility measured with a field of 0.5 T.

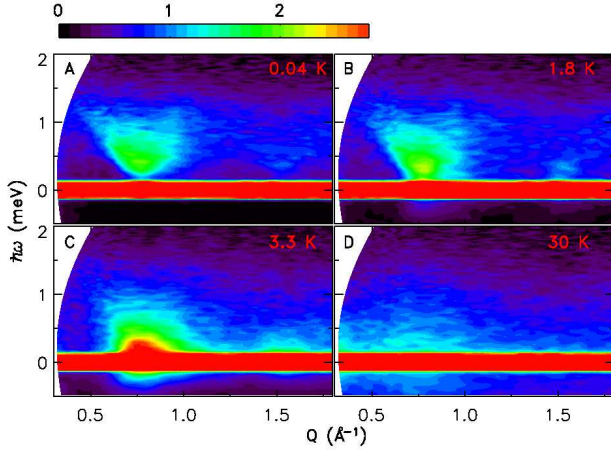


FIG. 2: (color online) Magnetic spectral function $S(\mathbf{Q}, \omega)$ measured at (a) 0.04 K, (b) 1.8 K, (c) 3.3 K and (d) 30 K. The intensity in a.u. is indicated by the color bar at the top.

measurements indicate a second-order phase transition at $T_N = 2.80 \text{ K} \ll |\Theta|$, which is accompanied by a small anomaly in magnetic susceptibility (Fig. 1c,d).

To further investigate the magnetic order and excitations, neutron scattering experiments were carried out using the Disk Chopper Time-of-Flight Spectrometer at NIST. The spectrometer simultaneously measures elastic and inelastic magnetic neutron scattering from the high purity polycrystalline sample of 4.7 g, which was encapsulated with He exchange gas in a copper cylinder in a dilution refrigerator. The selection of incident neutrons of 3.55 meV properly covers the spectral range of $\text{La}_2\text{Ca}_2\text{MnO}_7$ and yields an energy resolution of 0.13 meV at full-width-at-half-maximum (FWHM) for incoherent elastic scattering. A few representative spectra as a function of the wave-number Q and energy $\hbar\omega$ measured from 0.04 to 30 K are shown in Fig. 2.

Let us first examine elastic magnetic neutron scattering, which is at $\hbar\omega = 0$ part of the full spectrum in Fig. 2. Raw data measured at two temperatures, well below and above T_N , are shown in Supplementary Figure. While the temperature-independent 3D structural Bragg peaks are resolution-limited, the temperature-dependent magnetic signal shows the classic, asymmetric Warren peak profile from a 2D structure[20]. The integrated intensity from $Q = 0.5$ to 1 \AA^{-1} , covering the first Warren peak, is shown as a function of temperature in the inset to Fig. 3 by red circles, and resembles the typical order parameter of a second-order magnetic phase-transition. Extra intensity near T_N is due to the well-understood critical spin fluctuations, which peak at T_N . There is negligible magnetic elastic intensity left at 30 K, which spectrum can be used as background to isolate magnetic elastic neutron scattering intensity as shown in Fig. 3 at various temperatures.

The Warren peaks below T_N in Fig. 3 testify to 2D magnetic order in $\text{La}_2\text{Ca}_2\text{MnO}_7$. The characteristic difference in diffraction intensities between 2D and 3D order is that the latter produces discrete Bragg points in reciprocal space, while Bragg points coalesce into continuous lines for 2D order. Therefore, for 2D $\sqrt{3} \times \sqrt{3}$ order, the powder diffraction intensity is[20]

$$I(Q) = A \left(\frac{f(Q)}{\sin 2\theta} \right)^2 \sum_i \frac{n_i Q |F(\mathbf{q}_i)|^2}{\sqrt{Q^2 - q_i^2}} \Theta(Q - q_i), \quad (1)$$

where A is a constant, $f(Q)$ the atomic form factor, $1/\sin^2 2\theta$ the usual Lorentz factor, n_i the multiplicity of a Bragg peak, and $|F(\mathbf{q})|^2$ the squared magnetic structure factor at the 2D Bragg points of the $\sqrt{3} \times \sqrt{3}$ order. The unit step function $\Theta(x)$ ensures that the Warren profile function $Q/\sqrt{Q^2 - q_i^2}$ is real, which replaces the delta function in 3D powder diffraction. The solid line

through the measured data in Fig. 3 is Eq. (1) convoluted with the instrument resolution function. The 2D Warren peak profile describes excellently the asymmetric peaks at $q_0 = 4\pi/3a = 0.7455\text{\AA}^{-1}$ and $q_1 \equiv 8\pi/3a = 1.491\text{\AA}^{-1}$ from 40 mK to 1.8K. As a comparison, if $\text{La}_2\text{Ca}_2\text{MnO}_7$ developed a 3D magnetic order, such as that observed in CuCrO_2 [14], the peak profile would have been like those indicated by the red line in Fig. 3 with discrete peaks at $(1/3, 1/3, n)$ and $(2/3, 2/3, n)$, $n=0,1,2,3$. At 2.6 and 3.3 K, the measured spectra are broadened, which can be attributed to critical spin fluctuations in the vicinity of T_N . Thus, our elastic neutron scattering results clearly demonstrate that the $\sqrt{3} \times \sqrt{3}$ order in $\text{La}_2\text{Ca}_2\text{MnO}_7$ remains 2D down to 40 mK.

The 2D nature of the $\sqrt{3} \times \sqrt{3}$ order in $\text{La}_2\text{Ca}_2\text{MnO}_7$ is also corroborated in the spin dynamics. In Fig. 2d, spin excitations are noticeable well above T_N at 30 K. With decreasing temperature, the intensity grows and coalesces only at the 2D Bragg wave-vectors at $Q = q_0$ and q_1 (Fig. 2c). With further cooling below T_N , the spectral weight of low-energy spin excitations moves progressively to the static order, and a cone-shaped spectral distribution takes shape at q_0 and q_1 (Fig. 2a,b). If 3D magnetic order developed in $\text{La}_2\text{Ca}_2\text{MnO}_7$, the spin excitation cones would appear also at those extra 3D Bragg spots $(1/3, 1/3, n)$ and $(2/3, 2/3, n)$.

In previous neutron powder diffraction studies, 2D Warren magnetic peaks have been observed at finite temperature for square-lattice Ising antiferromagnets[21], consistent with theoretical expectations[4]. Such antiferromagnetic order however is impossible on the triangular lattice due to geometric frustration[3]. The existence of $\sqrt{3} \times \sqrt{3}$ order in $\text{La}_2\text{Ca}_2\text{MnO}_7$ further shows that its spins are not Ising-like: they can rotate to form the non-collinear three-sublattice order. The question is how can the 2D $\sqrt{3} \times \sqrt{3}$ order in $\text{La}_2\text{Ca}_2\text{MnO}_7$ have a phase transition at finite T_N , in apparent defiance of the Mermin-Wagner theorem?

One possibility proposed in previous theoretical studies invokes the topological character of the $\sqrt{3} \times \sqrt{3}$ order, namely chirality, which is absent for classic bipartite Néel order[22]. With its Ising-like symmetry, chiral long-range order has been predicted theoretically for the TAF at finite temperature[22], but never before observed in a continuous-symmetry system. An open theoretical question is whether chiral long-range order would push the spin state to a long-range order at finite temperature, given that the Kosterlitz-Thouless state at finite temperature is already power-law critical without the chirality. Another, more conventional, possibility is the breaking of continuous symmetry in spin space with a finite 3-state Potts anisotropy, which is symmetry-allowed by the triple ligand environment of Mn^{4+} and typical ligand-field energy splittings for octahedrally-coordinated Mn^{4+} are of order 10^{-2} meV, much smaller than the energy resolution of our cold neutron spectrometer. It is important to

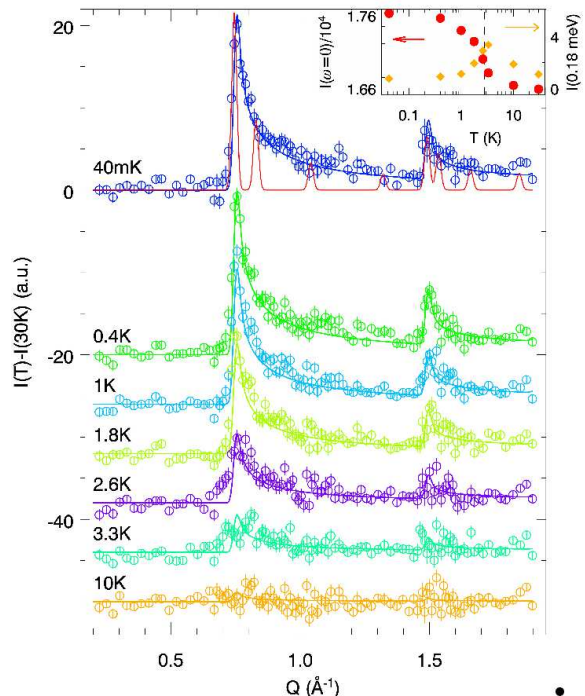


FIG. 3: (color online) The Warren peaks of 2D $\sqrt{3} \times \sqrt{3}$ spin order in $\text{La}_2\text{Ca}_2\text{MnO}_7$ at various temperatures. The solid lines are resolution-convoluted fit to Eq. (1). The red line indicates the resolution-convoluted Bragg peaks when the $\sqrt{3} \times \sqrt{3}$ order in different triangular layers form a 3D antiferromagnetic order[14]. The zeros of the spectra at $T \geq 0.4$ K have been shifted down for clarity. Inset: Elastic magnetic intensity (red circles) and the intensity of critical spin fluctuations measured at 0.18 meV and q_0 (orange diamond) as a function of temperature. The dashed line marks $T_N = 2.8$ K.

note that the Potts-type order has not been previously observed in a material without 3D correlations driving the ordering.

Now let us examine the observed spin excitations from the 2D $\sqrt{3} \times \sqrt{3}$ ground state. The cone-shaped spectra at magnetic Bragg reflection q_0 in Fig. 2a indicate that magnetic spectral weight in $\text{La}_2\text{Ca}_2\text{MnO}_7$ exists within the spin-wave cone defined by $\hbar\omega(\mathbf{q}) = \hbar c\mathbf{q}$ at low temperatures. The slope of the front locus of the intensity distribution at $Q \leq q_0$ measures the spin-wave velocity c , and it is consistent with the linear spin-wave theory prediction[23] $c = (3/2)^{3/2} J S a \approx 4.5 \text{ meV}\text{\AA}$, using $J = 0.29 \text{ meV}$ from the Rushbrooke-Wood fit to our measured susceptibility. The consistency between the static magnetic susceptibility and the dynamic excitation spectrum indicates that $\text{La}_2\text{Ca}_2\text{MnO}_7$ indeed is an excellent material realization of the nearest-neighbor antiferromagnet on the triangular lattice.

Unlike previous studies of quasi-2D TAFs that ultimately exhibit 3D order and have excitations given by linear spin-wave theory (LSWT)[24], such theory completely fails to describe the intensity distribution in

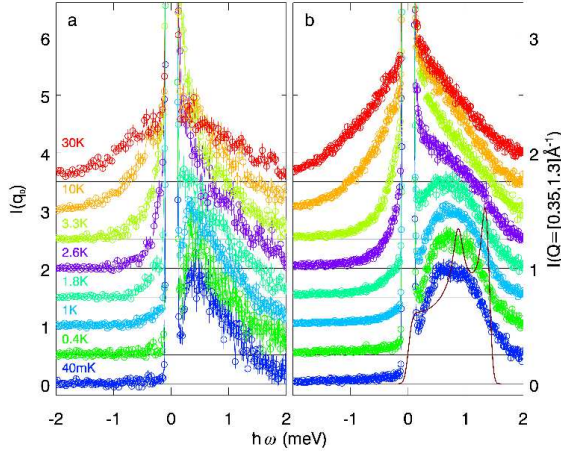


FIG. 4: (color online) (a) The powder energy spectra of spin excitations at the Bragg wave-number q_0 . (b) The magnetic density-of-states $\int dQ S(\mathbf{Q}, \omega)$. The red curve represents the predication of linear spin-wave theory[23]. The same color is used in (a) and (b) to indicate the same measurement temperature. The zeros of spectra taken at $T \geq 0.4$ K, indicated by the horizontal lines, have been shifted up for clarity.

$\text{La}_2\text{Ca}_2\text{MnO}_7$. The LSWT magnetic density-of-states (MDOS) at zero temperature is readily available[23] and is shown after resolution convolution as the red curve in Fig. 4b to be compared with experimental MDOS at 40 mK obtained by integrating intensity from $Q = 0.35$ to 1.3\AA^{-1} , which includes most of the spectral weight in the first Brillouin zone (Fig. 2). This failure is anticipated by recent quantum theoretical works which show that magnons are not elementary excitation modes at higher energy, even though the low energy cone-shaped part remains[23]. In general, the energy scales for the saddle point and the spin-wave bandwidth are substantially renormalized downward in the series expansions and the $1/S$ expansion studies. But our observation of the existence of magnetic excitations above the spin-wave bandwidth $\sqrt{10}JS = 1.3$ meV is not anticipated in these theories. Both multi-magnon decay and spinon-pair excitations have been proposed[23] but the spectral function $S(\mathbf{Q}, \omega)$ has yet to be calculated for experimental verification. For future comparison, we provide spin excitation spectra at $Q = q_0$ in Fig. 4a and MDOS in Fig. 4b at various temperatures.

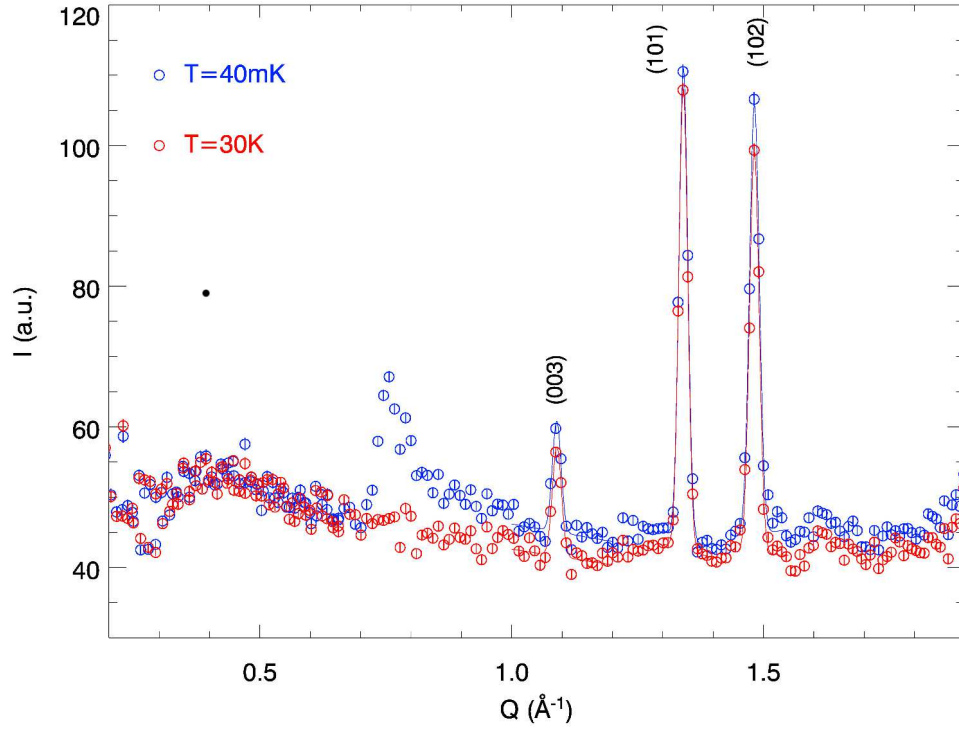
In summary, we report two-dimensional $\sqrt{3} \times \sqrt{3}$ spin order existing from $T_N = 2.80$ K down to 40 mK in $\text{La}_2\text{Ca}_2\text{MnO}_7$. This allows us to investigate spin excitations from the 2D ground state of a TAF. The spin-wave dispersion relation for low-energy spin excitations, which survives quantum corrections, is supported by our data. The spectral weight distribution and bandwidth of spin excitations, however, are yet to be accounted for by theory. Thus $\text{La}_2\text{Ca}_2\text{MnO}_7$ represents a new model material for the study of quantum antiferromagnetism.

We thank R.R.P. Singh, Y. Ran, D.H. Lee, A. Läuchli, O. Tchernyshyov, I.A. Zaliznyak, Z. Nussinov, C. Broholm, B. Normand, O.P. Sushkov, A.V. Chubukov and R.H. McKenzie for stimulating discussions. Works at Peking University were supported by National Natural Science Foundation of China (NSFC 20571004 and 20531010), and the DCS was partially funded by NSF (Agreement No. DMR-0454672).

* Electronic address: wbao@ruc.edu.cn

† Electronic address: wangyx@pku.edu.cn

- [1] R. Kubo, Phys. Rev. **568**, 87 (1952).
- [2] I. Affleck, J. Phys. Condens. Matter **1**, 3047 (1989).
- [3] A. P. Ramirez, in *Handbook of Magnetic Materials*, edited by K.J.H. Buschow (Elsevier Science, Amsterdam, 2001).
- [4] L. Onsager, Phys. Rev. **65**, 117 (1944).
- [5] N. D. Mermin and H. Wagner, Phys. Rev. Lett. **17**, 1133 (1966).
- [6] J. M. Kosterlitz and D. Thouless, J. Phys. C **6**, 1181 (1973); J. M. Kosterlitz, J. Phys. C **7**, 1046 (1974).
- [7] D. A. Huse and V. Elser, Phys. Rev. Lett. **60**, 2531 (1988).
- [8] P. Fazekas and P. W. Anderson, Philos. Mag. **30**, 432 (1974).
- [9] J. Villain, J. Phys. (Paris) **38**, 385 (1977).
- [10] R. R. P. Singh and D. A. Huse, Phys. Rev. Lett. **68**, 1766 (1992); P. W. Leung and K. J. Runge, Phys. Rev. B **47**, 5861 (1992); T. Jolicoeur and J. C. L. Guillou, ibid **40**, 2727 (1989).
- [11] M. F. Collins and O. A. Petrenko, Can. J. Phys. **75**, 605 (1997).
- [12] A. E. Trumper, Phys. Rev. B **60**, 2987 (1999); W. LiMing et al., ibid **62**, 6372 (2000); S. Nakatsuji et al., Science **309**, 1697 (2005); H. Tsunetsugu and M. Arikawa, J. Phys. Soc. Jpn. **75**, 083701 (2006); A. Läuchli et al., Phys. Rev. Lett. **97**, 087205 (2006).
- [13] K. Hirakawa et al., J. Phys. Soc. Jpn. **52**, 1814 (1983).
- [14] H. Kadowaki et al., J. Phys.: Condens. Matter **2**, 4485 (1990).
- [15] J. L. Soubeyroux et al., J. Magn. Magn. Mater. **14**, 159 (1979); H. Kadowaki et al., J. Phys.: Condens. Matter **7**, 6869 (1995).
- [16] H. Serrano-González et al., Phys. Rev. B **59**, 14451 (1999).
- [17] L. E. Svistov et al., Phys. Rev. B **74**, 024412 (2006).
- [18] Y.-X. Wang et al., J. Solid State Chem. **177**, 65 (2004).
- [19] G. S. Rushbrooke and P. J. Wood, Molec. Phys. **6**, 409 (1963).
- [20] B. E. Warren, Phys. Rev. **59**, 693 (1941).
- [21] J. W. Lynn, J. Alloys Comp. **181**, 419 (1992).
- [22] D. H. Lee et al., Phys. Rev. Lett. **52**, 433 (1984); H. Kawamura and S. Miyashita, J. Phys. Soc. Jpn. **53**, 4138 (1984); N. Suzuki and F. Matsubara, Phys. Rev. B **55**, 12331 (1997).
- [23] W. Zheng et al., Phys. Rev. Lett. **96**, 057201 (2006); A. L. Chernyshev and M. E. Zhitomirsky, ibid **97**, 207202 (2006); O. A. Starykh et al., Phys. Rev. B **74**, 180403(R) (2006).
- [24] T. J. Sato et al., Phys. Rev. B **68**, 014432 (2003).



Supplementary Figure 1: Elastic neutron scattering spectrum of $\text{La}_2\text{Ca}_2\text{MnO}_7$ at 0.04 (blue) and 30 (red) K. The three-dimensional structural Bragg peaks (003), (101) and (102) are resolution-limited. Their integrated intensities are temperature independent. The two-dimensional magnetic peak at $q_0 = 0.7455\text{\AA}^{-1}$ has the asymmetric Warren profile. The magnetic peak at $q_1 = 1.491\text{\AA}^{-1}$ is obscured by the (102), and is revealed in the difference plot in Fig. 3.